B.M. LISNYI

Institute for Condensed Matter Physics, Nat. Acad. of Sci. of Ukraine
(1, Svientsitskii Str., Lviv 79011, Ukraine; e-mail: lisnyj@icmp.lviv.ua)

DISTORTED DIAMOND ISING–HUBBARD CHAIN IN THE SPECIAL LIMIT OF INFINITE ON-SITE REPULSION

The exact solution of the distorted diamond Ising–Hubbard chain is analyzed in the special limit of infinite on-site electron-electron repulsion, where the two-electron Hubbard dimer becomes equivalent to the antiferromagnetic isotropic Heisenberg dimer. The special limit of infinite repulsion for the matrix of the cell Hamiltonian of this model is analytically calculated, and it is demonstrated that the exact solution of the distorted diamond Ising–Hubbard chain in this limit coincides with the exact solution of the spin-1/2 distorted diamond Ising–Heisenberg chain with antiferromagnetic isotropic Heisenberg interaction. The numerical calculation of the special limit of infinite repulsion for the ground-state phase diagram and thermodynamic characteristics of the distorted diamond Ising–Hubbard chain was performed in a way that provides a very fast convergence to the limit results for these characteristics.

K e y w o r d s: Ising–Hubbard diamond chain, exact solution, ground state, thermodynamic characteristics, geometric frustration.

1. Introduction

Interest in studying the ground state, magnetic and thermal properties, and, lately, pseudocritical behavior of the spin-1/2 diamond Ising–Heisenberg chain [1–16] and the spin-electron diamond Ising–Hubbard chain [17–22] is largely initiated by the unusual features of the magnetic and thermal properties of the natural mineral azurite $Cu_3(CO_3)_2(OH)_2$, such as the presence of a plateau at one-third of the saturation magnetization in the magnetization curve at low temperature and the presence of two peaks in the temperature dependence of the specific heat [23–26]. Azurite is known to provide an experimental realization of the frustrated spin-1/2 diamond Heisenberg chain [27, 28]. Although the exactly solvable spin-1/2 diamond Ising–Heisenberg chain [1, 2, 11] yields only a simplified version of the aforementioned model, it qualitatively reproduces the experimental features of magnetization and specific heat of azurite: an in-

termediate one-third magnetization plateau and the double-peak temperature dependence of specific heat [23–26]. Therefore, the theoretical study of the spin-1/2 diamond Ising–Heisenberg [1–16] and Ising–Hubbard [17–22] chains is a useful playground for understanding the mechanisms of formation of intermediate plateaus in the magnetization curve and additional maxima in the temperature curve of specific heat, as well as for analizing the influence of geometric frustration and quantum fluctuations. These relatively simple models can be also used to study more complex systems using the many-body perturbation theory [29, 30].

The ground-state phase diagrams, magnetization curves, temperature curves of magnetization, magnetic susceptibility, and specific heat of spin-1/2 antiferromagnetic distorted diamond chains of Ising–Hubbard [19] and Ising–Heisenberg [2] are very similar to each other. This similarity is not accidental, because the Hubbard model for two electrons on a two-node cluster (dimer) with very strong on-site electron-electron repulsion in the second order of expansion by the hopping integral is equivalent to the antiferromagnetic isotropic (XXX) Heisenberg model on a spin-1/2 two-node cluster [31, 32]. In the special limit of infinite on-site repulsion, which preserves the spe-

cial ratio between on-site repulsion and the hopping integral, the expansion by the hopping integral [31,32] contains only the second order, and the higher orders turn to zero. Therefore, the two-electron Hubbard dimer in this special limit of infinite repulsion is equivalent to the spin-1/2 antiferromagnetic *XXX* Heisenberg dimer. Near this special limit, there is a qualitative and quantitative interrelation between the quantum mechanical, magnetic, and thermal characteristics of the diamond chains Ising–Hubbard [19] and Ising–Heisenberg [2] (with the antiferromagnetic isotropic Heisenberg interaction). The study of this interrelation will make it possible to predict the behavior and calculate the physical characteristics of Ising models decorated with spin-1/2 antiferromagnetic Heisenberg dimers, based on the results for the physical characteristics of the corresponding Ising models decorated with two-electron Hubbard dimers, and vice versa.

The paper considers the special limit of infinite on-site electron-electron repulsion, in which the two-electron Hubbard dimer is equivalent to the antiferromagnetic isotropic Heisenberg dimer, for the ground state and the exact solution of the distorted diamond Ising–Hubbard chain. We will analytically demonstrate that the quantum mechanical states and the exact solution of the distorted diamond Ising–Hubbard chain in this special limit and the spin-1/2 distorted diamond Ising–Hubbard chain with antiferromagnetic *XXX* Heisenberg interaction are equivalent among themselves. We also will obtain the special limit of infinite on-site electron-electron repulsion for the ground-state phase diagram, magnetic and thermal characteristics of the distorted diamond Ising–Hubbard chain in the case of antiferromagnetic Ising interaction by a numerical method that ensures very fast convergence to the results of the special limit for these characteristics. In this way, we will calculate the ground state phase diagram, magnetic and thermal characteristics of the spin-1/2 distorted diamond Ising–Heisenberg chain in the case of antiferromagnetic interactions: Ising and *XXX* Heisenberg.

2. Special Limit of Infinite on-Site Repulsion for Exact Solution of the Model

Let us consider the distorted diamond Ising–Hubbard chain in an external magnetic field [19]. The primitive cell of the chain (Fig. 1) contains nodes i and $i+1$ and interstitial positions $(i, 1)$ and $(i, 2)$. Nodes i are occu-
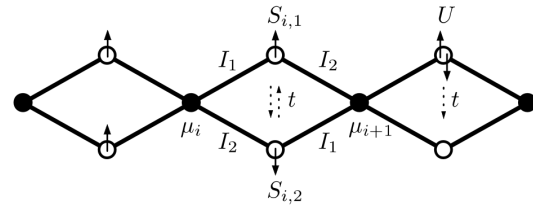

Fig. 1. Schematic diagram of a fragment from the distorted diamond Ising–Hubbard chain. Solid and hollow circles denote nodes occupied by Ising spins and interstitial positions occupied by mobile electrons, respectively

pied by Ising spins $\mu_i = \pm 1/2$, which are coupled with neighbor spins by means of the Ising interaction. At the interstitial positions $(i, 1)$ and $(i, 2)$ there are two mobile electrons with the on-site repulsion between them, which hop between these interstitial positions according to Pauli's rule. Thus, interstitial positions $(i, 1)$ and $(i, 2)$ form a Hubbard dimer half-filled by electrons.

The Hamiltonian of this chain $\mathcal{H}$ is the sum of the cell Hamiltonians $\mathcal{H}_i$ [19]:

$$
\begin{aligned}
\mathcal{H} &= \sum_{i=1}^{N} \mathcal{H}_i, \\
\mathcal{H}_i &= \sum_{\sigma \in \{\uparrow, \downarrow\}} t(c_{i,1;\sigma}^\dagger c_{i,2;\sigma} + c_{i,2;\sigma}^\dagger c_{i,1;\sigma}) + \\
&+ \sum_{d=1}^{2} U c_{i,d;\uparrow}^\dagger c_{i,d;\uparrow} c_{i,d;\downarrow}^\dagger c_{i,d;\downarrow} + \\
&+ \mu_i(I_1 S_{i,1} + I_2 S_{i,2}) + \mu_{i+1}(I_2 S_{i,1} + I_1 S_{i,2}) - \\
&- \frac{1}{2} h_1(\mu_i + \mu_{i+1}) - h_2(S_{i,1} + S_{i,2}),
\end{aligned}
\tag{1}
$$

where N is the number of primitive cells in the chain; $c_{i,d;\sigma}^\dagger$ and $c_{i,d;\sigma}$ are the creation and annihilation operators for an electron with spin $\sigma \in \{\uparrow, \downarrow\}$ at interstitial position (i, d); μ_i is the z-component of the spin-1/2 operator at node i, for which the periodic boundary condition $\mu_{N+1} \equiv \mu_1$ is implied; $S_{i,d} = (c_{i,d;\uparrow}^\dagger c_{i,d;\uparrow} - c_{i,d;\downarrow}^\dagger c_{i,d;\downarrow})/2$ is the z-component of the operator for the total spin of the electrons at interstitial position (i, d); the parameters t and U denote the hopping integral and the on-site Coulomb repulsion of the electrons; I_1 and I_2 are the parameters of the Ising coupling for the bonds along the diamond sides (Fig. 1), which are identical only for collinear bonds; h_1 and h_2 are magnetic fields that act on Ising spins and electron spins, respectively. It should

be noted that Hamiltonian (1) also corresponds to a simple Ising–Hubbard chain (the nodes and interstitial positions are located on the line), in which the Ising spin μ_i is coupled with the first, I_1, and second, I_2, neighbors.

The partition function of the distorted diamond Ising–Hubbard chain $\mathcal{Z} = \mathrm{Tr} \exp(-\beta \mathcal{H})$, where $\beta = 1/k_{\mathrm{B}}T$, k_{B} is the Boltzmann constant, and T is the absolute temperature, is reduced to the form [19]

$$\mathcal{Z} = \mathrm{Tr}_{\{\mu\}} \prod_{i=1}^{N} \mathrm{Tr}_{\{i,1;i,2\}} \exp(-\beta \mathcal{H}_i),$$

where $\mathrm{Tr}_{\{\mu\}}$ is the trace with respect to the Ising spins and $\mathrm{Tr}_{\{i,1;i,2\}}$ is the trace with respect to the states of two electrons at positions $(i,1)$ and $(i,2)$. In order to obtain an exact solution and to determine the ground state of this model, it is necessary to get the eigenvalues and eigenfunctions of the cell Hamiltonian $\mathcal{H}_i$ (1). The exact solution and ground state of this model were obtained earlier in paper [19]. Here, we will find the matrix and eigenvalues of the cell Hamiltonian $\mathcal{H}_i$ in the limit $U \to \infty$ with the condition $4t^2/U = J$, where J is a positive parameter, that is, in the limit $(t \to \infty, U \to \infty)|_{4t^2/U=J}$. In this special limit $U \to \infty$, which preserves the special ratio between the on-site repulsion and the hopping integral, the two-electron Hubbard dimer is equivalent to the spin-1/2 antiferromagnetic *XXX* Heisenberg dimer.

Let us move on to the matrix representation of the Hamiltonian $\mathcal{H}_i$ in the subspace of the electron states. To do this, we take a basis constructed from the states of two electrons in the ith diamond cell [19]:

$$|\uparrow, \uparrow\rangle_i = c^\dagger_{i,1;\uparrow} c^\dagger_{i,2;\uparrow}|0\rangle, \quad |\downarrow, \downarrow\rangle_i = c^\dagger_{i,1;\downarrow} c^\dagger_{i,2;\downarrow}|0\rangle,$$

$$|\uparrow, \downarrow\rangle_i = c^\dagger_{i,1;\uparrow} c^\dagger_{i,2;\downarrow}|0\rangle, \quad |\downarrow, \uparrow\rangle_i = c^\dagger_{i,1;\downarrow} c^\dagger_{i,2;\uparrow}|0\rangle, \quad (2)$$

$$|\uparrow\downarrow, 0\rangle_i = c^\dagger_{i,1;\uparrow} c^\dagger_{i,1;\downarrow}|0\rangle, \quad |0, \uparrow\downarrow\rangle_i = c^\dagger_{i,2;\uparrow} c^\dagger_{i,2;\downarrow}|0\rangle.$$

In this basis, the Hamiltonian $\mathcal{H}_i$ can be presented in the following matrix form:

$$\mathbf{H}_i = \epsilon_1 \oplus (-\epsilon_1) \oplus \mathbf{K} - \frac{h_1}{2}(\mu_i + \mu_{i+1})\mathbf{1}, \quad (3)$$

where

$$\epsilon_1 = \frac{I_1 + I_2}{2}(\mu_i + \mu_{i+1}) - h_2,$$

$$\mathbf{K} = \begin{pmatrix} \epsilon_2 & 0 & t & t \\ 0 & -\epsilon_2 & -t & -t \\ t & -t & U & 0 \\ t & -t & 0 & U \end{pmatrix},$$

$$\epsilon_2 = \frac{I_1 - I_2}{2}(\mu_i - \mu_{i+1}),$$

and $\mathbf{1}$ is the unit matrix. The matrix $\mathbf{K}$ is invariant with respect to the permutation of the third and fourth rows/columns. This symmetry allows us to find a unitary transformation

$$\mathbf{P} = \begin{pmatrix} \frac{1}{\sqrt{2}} & -\frac{1}{\sqrt{2}} \\ \frac{1}{\sqrt{2}} & -\frac{1}{\sqrt{2}} \end{pmatrix} \oplus \begin{pmatrix} \frac{1}{\sqrt{2}} & -\frac{1}{\sqrt{2}} \\ \frac{1}{\sqrt{2}} & -\frac{1}{\sqrt{2}} \end{pmatrix}, \quad (4)$$

which reduces the matrix $\mathbf{K}$ to a quasi-diagonal form

$$\mathbf{K}_1 = \mathbf{P}^+ \mathbf{K} \mathbf{P} = \mathbf{L} \oplus U, \quad (5)$$

where

$$\mathbf{L} = \begin{pmatrix} 0 & \epsilon_2 & 0 \\ \epsilon_2 & 0 & 2t \\ 0 & 2t & U \end{pmatrix}.$$

So, now we need to find the special limit $U \to \infty$ for the matrix $\mathbf{L}$. To do this, we write the matrix $\mathbf{L}$ as a sum of two matrices:

$$\mathbf{L} = \mathbf{L}_0 + \epsilon_2 \begin{pmatrix} 0 & 1 & 0 \\ 1 & 0 & 0 \\ 0 & 0 & 0 \end{pmatrix},$$

where

$$\mathbf{L}_0 = \begin{pmatrix} 0 & 0 & 0 \\ 0 & 0 & 2t \\ 0 & 2t & U \end{pmatrix}.$$

Thus, we separated the contributions from the two-electron Hubbard dimer and from the Ising bonds along the sides of the diamond cell. Now, we focus on the matrix $\mathbf{L}_0$, which contains the parameters t and U, for which we need to go to the limit $(t \to \infty, U \to \infty)|_{4t^2/U=J}$. We find the eigenvalues of the matrix $\mathbf{L}_0$:

$$l_1 = 0, \quad l_{2,3} = \frac{1}{2}\left(U \mp \sqrt{U^2 + 16t^2}\right),$$

and their corresponding eigenvectors, on the basis of which we obtain the unitary transformation

$$\mathbf{Q} = \begin{pmatrix} 1 & 0 & 0 \\ 0 & q_2 & q_3 \\ 0 & -q_3 & q_2 \end{pmatrix}, \quad q_{2,3} = \frac{1}{\sqrt{2}}\sqrt{1 \pm \frac{U}{\sqrt{U^2 + 16t^2}}},$$

which realizes the transition to the basis formed from the eigenvectors of the matrix $\mathbf{L}_0$. Now, we apply the unitary transformation $\mathbf{Q}$ to the matrix $\mathbf{L}$ and obtain it in the following form:

$$\mathbf{L}_1 = \mathbf{Q}^+ \mathbf{L} \mathbf{Q} = \begin{pmatrix} 0 & 0 & 0 \\ 0 & l_2 & 0 \\ 0 & 0 & l_3 \end{pmatrix} + \epsilon_2 \begin{pmatrix} 0 & q_2 & q_3 \\ q_2 & 0 & 0 \\ q_3 & 0 & 0 \end{pmatrix}.$$

Let us find the matrix $\mathbf{L}_1$ in the special limit $U \to \infty$. To do this, we find the eigenvalues of l_2, l_3 and elements q_2 and q_3 of the matrix $\mathbf{Q}$ in the limit $(t \to \infty, U \to \infty)|_{4t^2/U=J}$:

$$\lim_{U \to \infty} l_2 = -J, \lim_{U \to \infty} l_3 = \infty, \lim_{U \to \infty} q_2 = 1, \lim_{U \to \infty} q_3 = 0.$$

Using these results, we obtain the matrices $\mathbf{Q}$, $\mathbf{L}_1$, and $\mathbf{L}$ in the special limit $U \to \infty$: $\lim_{U \to \infty} \mathbf{Q} = \mathbf{1}$,

$$\lim_{U \to \infty} \mathbf{L}_1 = \lim_{U \to \infty} \mathbf{L} = \begin{pmatrix} 0 & \epsilon_2 & 0 \\ \epsilon_2 & -J & 0 \\ 0 & 0 & \infty \end{pmatrix}.$$

Now, we get the matrix $\mathbf{K}_1$ (5) in the special limit $U \to \infty$:

$$\mathbf{K}_{1\infty} = \lim_{U \to \infty} \mathbf{K}_1 = \begin{pmatrix} 0 & \epsilon_2 \\ \epsilon_2 & -J \end{pmatrix} \oplus \begin{pmatrix} \infty & 0 \\ 0 & \infty \end{pmatrix}.$$

To return to the basis vectors $|\uparrow, \downarrow\rangle_i$ and $|\downarrow, \uparrow\rangle_i$ (see Eqs. (2)), we apply the unitary transformation

$$\mathbf{R} = \begin{pmatrix} \frac{1}{\sqrt{2}} & \frac{1}{\sqrt{2}} \\ \frac{1}{\sqrt{2}} & -\frac{1}{\sqrt{2}} \end{pmatrix} \oplus \begin{pmatrix} 1 & 0 \\ 0 & 1 \end{pmatrix},$$

which neutralizes the action of the first block of the unitary transformation $\mathbf{P}$ (4), to the matrix $\mathbf{K}_{1\infty}$. As a result of a series of successive operations on the matrix $\mathbf{K}$ (3) – the unitary transformation $\mathbf{P}$, the transition to the special limit $U \to \infty$, and the unitary transformation $\mathbf{R}$ – we obtain the matrix $\mathbf{H}_i$ (3) of the cell Hamiltonian $\mathcal{H}_i$ in the special limit $U \to \infty$

$$\mathbf{H}'_i = \epsilon_1 \oplus (-\epsilon_1) \oplus \begin{pmatrix} \epsilon_2 - \frac{J}{2} & \frac{J}{2} \\ \frac{J}{2} & -\epsilon_2 - \frac{J}{2} \end{pmatrix} \oplus \begin{pmatrix} \infty & 0 \\ 0 & \infty \end{pmatrix} - \\ - \frac{h_1}{2}(\mu_i + \mu_{i+1})\mathbf{1}. \quad (6)$$

If we add the constant $(J/4)\mathbf{1}$ to matrix $\mathbf{H}'_i$ and discard two one-dimensional subspaces with infinite eigenvalues, then we get the matrix of the cell Hamiltonian of the spin-1/2 distorted diamond Ising–Heisenberg chain with the antiferromagnetic isotropic

Heisenberg interaction J [2]. Note that the infinitely large energies of the Hamiltonian $\mathbf{H}'_i$ do not influence the thermodynamics of this system in the region of finite temperatures, because they are unattainable for finite thermal excitations. Therefore, the Hamiltonian of the distorted diamond Ising–Hubbard chain in the special limit $U \to \infty$ is equivalent to the Hamiltonian of the spin-1/2 distorted diamond Ising–Heisenberg chain with the antiferromagnetic isotropic Heisenberg interaction J [2]. Thus, the ground state and thermodynamic characteristics, except the free energy, of the distorted diamond Ising–Hubbard chain [19] in the special limit $U \to \infty$ coincide with the ground state and the corresponding thermodynamic characteristics of the spin-1/2 distorted diamond Ising–Heisenberg chain [2] with the antiferromagnetic isotropic Heisenberg interaction. The free energy of the given Ising–Hubbard chain per unit cell is smaller than the corresponding free energy of the Ising–Heisenberg chain by the constant $J/4$.

The matrix $\mathbf{H}'_i$ (6) has the following eigenvalues:

$$\mathcal{E}'_1(\mu_i, \mu_{i+1}) = \epsilon_1 - \frac{h_1}{2}(\mu_i + \mu_{i+1}),$$

$$\mathcal{E}'_2(\mu_i, \mu_{i+1}) = -\epsilon_1 - \frac{h_1}{2}(\mu_i + \mu_{i+1}),$$

$$\mathcal{E}'_3(\mu_i, \mu_{i+1}) = -\frac{J}{2} - \sqrt{\frac{J^2}{4} + \epsilon_2^2} - \frac{h_1}{2}(\mu_i + \mu_{i+1}),$$

$$\mathcal{E}'_4(\mu_i, \mu_{i+1}) = -\frac{J}{2} + \sqrt{\frac{J^2}{4} + \epsilon_2^2} - \frac{h_1}{2}(\mu_i + \mu_{i+1}),$$

$$\mathcal{E}'_5(\mu_i, \mu_{i+1}) = \infty - \frac{h_1}{2}(\mu_i + \mu_{i+1}),$$

$$\mathcal{E}'_6(\mu_i, \mu_{i+1}) = \infty - \frac{h_1}{2}(\mu_i + \mu_{i+1}).$$

$$(7)$$

The values of $\mathcal{E}'_k(\mu_i, \mu_{i+1}) + J/4$, where $k = \overline{1,4}$, coincide with the corresponding eigenvalues of the cell Hamiltonian of the spin-1/2 distorted diamond Ising–Heisenberg chain with the antiferromagnetic isotropic Heisenberg interaction J [2].

3. Numerical Calculation of the Special Limit $U \to \infty$ for the Ground State Phase Diagram and Thermodynamic Characteristics

Let us consider the numerical method of calculating the special limit $U \to \infty$ for the ground state phase diagram and thermodynamic characteristics, using

the analytic results for them from work [19]. The limit point $(t \to \infty, U \to \infty)|_{4t^2/U=J}$ can be reached along the curve $\xi(t, U) = 0$, which satisfies the equality $\lim_{U \to \infty} \xi(t, U) = a \lim_{U \to \infty} t^2/U - b$, where a and b are non-zero positive coefficients that satisfy the relation $J = 4b/a$. We find such a curve leading to the special limit $U \to \infty$, which reveals a very strong qualitative and quantitative connection between the ground state phase diagrams and thermodynamic characteristics of the distorted diamond Ising–Hubbard chain in wide ranges of t and U parameter values and the spin-1/2 distorted diamond Ising–Heisenberg chain with antiferromagnetic isotropic Heisenberg interaction J.

First, let us briefly recall the properties of the distorted diamond Ising–Hubbard chain in the ground state, which were studied in detail in work [19]. We consider the case of the antiferromagnetic Ising interaction on bonds in the diamond cell ($I_1 > 0, I_2 \geqslant 0$). In this case, the chain has geometric frustration, since the electron hopping is possible only with antiferromagnetic ordering of electron spins at different interstitial positions. Without loss of generality, we take $I_1 \geqslant I_2$ and introduce the parameter $\delta = I_1 - I_2$. We consider the case where the magnetic fields h_1 and h_2 are the same: $h = h_1 = h_2$. Let us move on to the dimensionless parameters

$$\tilde{t} = \frac{t}{I_1}, \quad \tilde{U} = \frac{U}{I_1}, \quad \tilde{\delta} = \frac{\delta}{I_1}, \quad \tilde{h} = \frac{h}{I_1}.$$

The parameter $\tilde{\delta} \in [0, 1]$ characterizes the degree of distortion of the diamond cell. In the system of dimensionless parameters, the definition of the special boundary $\tilde{U} \to \infty$ has the form $(\tilde{t} \to \infty, \tilde{U} \to \infty)|_{4\tilde{t}^2/\tilde{U}=\tilde{J}}$, where $\tilde{J} = J/I_1$ is dimensionless parameter of the antiferromagnetic Heisenberg interaction.

The model has four ground states [19]: the fully magnetized (FM) state, the ferrimagnetic (FRI) state, the monomer-dimer (MD) state, and the quantum antiferromagnetic (QAF) state. The energies of the states per primitive cell are [19]

$$\tilde{\mathcal{E}}_{\text{FM}} = 1 - \frac{\tilde{\delta}}{2} - \frac{3\tilde{h}}{2},$$
$$\tilde{\mathcal{E}}_{\text{FRI}} = -1 + \frac{\tilde{\delta}}{2} - \frac{\tilde{h}}{2},$$
$$\tilde{\mathcal{E}}_{\text{MD}} = \frac{1}{2}\left(\tilde{U} - \sqrt{\tilde{U}^2 + 16\tilde{t}^2}\right) - \frac{\tilde{h}}{2},$$
$$\tilde{\mathcal{E}}_{\text{QAF}} = \tilde{\Lambda}_0,$$

where $\tilde{\Lambda}_0$ is the lowest eigenvalue of the matrix $\tilde{\mathbf{L}} = \mathbf{L}/I_1$. These states correspond to the following wave functions [19]:

$$|\text{FM}\rangle = \prod_{i=1}^{N} |+\rangle_i |\uparrow, \uparrow\rangle_i,$$

$$|\text{FRI}\rangle = \prod_{i=1}^{N} |-\rangle_i |\uparrow, \uparrow\rangle_i,$$

$$|\text{MD}\rangle = \prod_{i=1}^{N} |+\rangle_i \left[\alpha_1\left(|\uparrow, \downarrow\rangle_i - |\downarrow, \uparrow\rangle_i\right) + \alpha_2 |\psi_i\rangle\right],$$

$$|\text{QAF}\rangle = \prod_{i=1}^{N} \left|(-)^{n=\left\{\begin{smallmatrix} i \\ i+1 \end{smallmatrix}\right\}}\right\rangle_i \times$$
$$\times \left(A_{(-)^n}|\uparrow, \downarrow\rangle_i - A_{(-)^{n+1}}|\downarrow, \uparrow\rangle_i + B|\psi_i\rangle\right),$$

where the functions $|\pm\rangle_i$ describe the states of the spins μ_i, $|\psi_i\rangle = |\uparrow\downarrow, 0\rangle_i + |0, \uparrow\downarrow\rangle_i$, the expression "$(-)^n$" means the sign of the number $(-1)^n$,

$$\alpha_{1,2} = \pm\frac{1}{2}\sqrt{1 \pm \frac{\tilde{U}}{\sqrt{\tilde{U}^2 + 16\tilde{t}^2}}},$$
$$A_\pm = \frac{\left(\tilde{\Lambda}_0 \pm \frac{1}{2}\tilde{\delta}\right)(\tilde{\Lambda}_0 - \tilde{U})}{\sqrt{2\Phi}}, \quad B = \frac{2\tilde{t}\tilde{\Lambda}_0}{\sqrt{2\Phi}},$$
$$\Phi = \left(\tilde{\Lambda}_0^2 + \frac{1}{4}\tilde{\delta}^2\right)(\tilde{\Lambda}_0 - \tilde{U})^2 + 4\tilde{t}^2\tilde{\Lambda}_0^2.$$

The magnetization $m = \langle \mu_i + S_{i,1} + S_{i,2}\rangle/3$ in these states has the following values: $m = m_{\text{sat}}$ in FM state, where $m_{\text{sat}} = 1/2$ is the saturation magnetization, $m = m_{\text{sat}}/3$ in FRI and MD states, $m = 0$ in QAF state.

From work [19], it is known that the topology of the ground state phase diagram in the plane $(\tilde{\delta}, \tilde{h})$ is determined by the topology parameter $(\tilde{\mathcal{T}})$

$$\tilde{\mathcal{T}} = \sqrt{\tilde{U}^2 + 16\tilde{t}^2} - \tilde{U}. \tag{8}$$

In the absence of the on-site repulsion ($U = 0$), the topology parameter $\tilde{\mathcal{T}}$ is determined by the following relation: $\tilde{\mathcal{T}} = 4\tilde{t}_0$, where $\tilde{t}_0 = t_0/I_1$, and t_0 is the hopping integral in the model without on-site electron repulsion. The ground state phase diagram in the plane $(\tilde{\delta}, \tilde{h})$ has three types of topology [19]. Figure 2 shows the second type of topology of the ground state phase diagram $(\tilde{\delta}, \tilde{h})$, which is realized under the condition $1 < \tilde{\mathcal{T}} < 2$ [19]. The regions of the FRI and MD

states in this phase diagram are separated by a segment on a vertical line $\tilde{\delta} = \tilde{\delta}_{\mathrm{F|M}} \equiv 2 - \tilde{\mathcal{T}}$. Recall that the ground state phase diagram $(\tilde{\delta}, \tilde{h})$ with the first type of topology is realized under the condition $\tilde{\mathcal{T}} \leqslant 1$. It looks the same as the fragment of the phase diagram in Fig. 2, which corresponds to the interval $\tilde{\delta} \in [0, \tilde{\delta}_{\mathrm{F|M}}]$ [19]. The third type of topology of the ground state phase diagram $(\tilde{\delta}, \tilde{h})$ is realized under the condition $2 \leqslant \tilde{\mathcal{T}}$. It generally corresponds to the fragment of the phase diagram in Fig. 2, which covers the interval $\tilde{\delta} \in [\tilde{\delta}_{\mathrm{F|M}}, 1]$, except that the line of coexistence of the QAF and MD ground states starts at the point $(0, 0)$ [19].

The dependence of the topology of the ground state phase diagram $(\tilde{\delta}, \tilde{h})$ on the parameters $\tilde{t}$ and $\tilde{U}$ can be represented using the topological diagram $(\tilde{t}, \tilde{U})$ [19], which is depicted in Fig. 3. The equitopological line (8), which starts at the point $(\tilde{t} = \tilde{t}_0, \tilde{U} = 0)$ and corresponds to topology parameter $\tilde{\mathcal{T}} = 4\tilde{t}_0$, is described by the equation

$$2\tilde{t}^2 - 2\tilde{t}_0^2 - \tilde{t}_0\tilde{U} = 0.$$

From this equation, we find that the equitopological line in the limit $\tilde{U} \to \infty$ satisfies the relation $\lim_{\tilde{U} \to \infty} 4\tilde{t}^2/\tilde{U} = 2\tilde{t}_0$. This means that the limit point $(\tilde{t} \to \infty, \tilde{U} \to \infty)$ on the equitopological line is a point of the special limit $\tilde{U} \to \infty$ and takes place equality $\tilde{J} = 2\tilde{t}_0 = \tilde{\mathcal{T}}/2$, which connects the parameter of the antiferromagnetic Heisenberg interaction with the hopping integral in the model without the on-site repulsion and with the topology parameter. Consequently, the equitopological line starts at the point $(\tilde{t} = \tilde{t}_0, \tilde{U} = 0)$, which corresponds to the model without the on-site electron repulsion, and ends at the point at infinity $(\tilde{t} \to \infty, \tilde{U} \to \infty)$, in which the two-electron Hubbard dimer is equivalent to the antiferromagnetic isotropic Heisenberg dimer with the interaction parameter $\tilde{J} = 2\tilde{t}_0 = \tilde{\mathcal{T}}/2$.

The energies of the FM, FRI, and MD states do not change along the equitopological line (8). Therefore the ground state phase diagram $(\tilde{\delta}, \tilde{h})$ changes the least (see Fig. 2) when changing of $\tilde{t}$ and $\tilde{U}$ along the equitopological line. In Fig. 2 we can see that, with the growth of $\tilde{U}$ along the equipotential line, the region of the QAF ground state expands, while the value of displacements of the lines of coexistence of states, that bound the region of the QAF ground state, rapidly decreases. In particular, the displace-
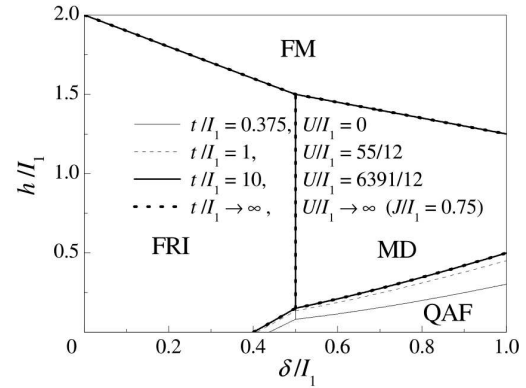
Fig. 2. Ground-state phase diagram in $(\tilde{\delta}, \tilde{h})$ plane. Lines of coexistence of ground states are shown for four sets of values of $\tilde{t}$ and $\tilde{U}$, which satisfy the condition $\tilde{\mathcal{T}} = 1.5$. In the case $\tilde{U} = 0$, the lines of coexistence are as in Ref. [17], and, in the case $\tilde{U} = 55/12$, they are as in Ref. [19]
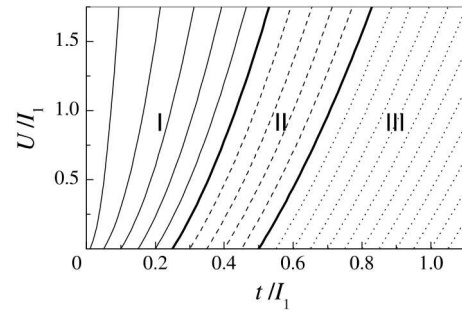

Fig. 3. Topological diagram $(\tilde{t}, \tilde{U})$ for the ground state phase diagram $(\tilde{\delta}, \tilde{h})$ [19]: equitopological lines $\tilde{\mathcal{T}}(\tilde{t}, \tilde{U}) = \mathrm{const}$ are shown here. The regions of three topologies, which are marked with numbers I, II, III, are separated by bold lines

ments of these lines due to the change of $\tilde{U}$ from 5 to 533 are about three times smaller than the corresponding displacements due to the change of $\tilde{U}$ from 0 to 5. The lines of state coexistence for $\tilde{U} = 533$ and for the limit $\tilde{U} \to \infty$ at $\tilde{J} = 0.75$ practically coincide with each other. Let us note that the ground state phase diagram in the special limit $\tilde{U} \to \infty$ was calculated using the energy spectrum (7). The zero temperature magnetization curve is determined from the ground state phase diagram $(\tilde{\delta}, \tilde{h})$. Therefore the change in this magnetization curve, which occurs along the equitopological line, is directly related to the above-considered changes in the phase diagram shown in Fig. 2.

Now, we compare, with each other, the thermodynamic characteristics for two points on the equi-
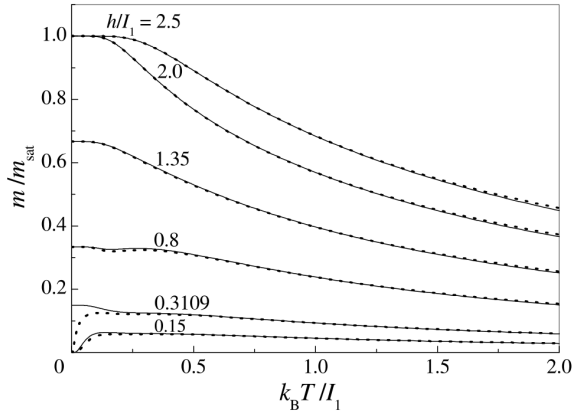
Fig. 4. The magnetization as a function of the temperature in the case of $\tilde{\delta} = 0.8$ for two points $(\tilde{t}, \tilde{U})$ and several selected values of the magnetic field. The results for $\tilde{t} = 1$ and $\tilde{U} = 55/12$ are depicted by solid lines, and the results for the special limit $\tilde{U} \to \infty$ ($\tilde{J} = 0.75$) is shown by dotted lines
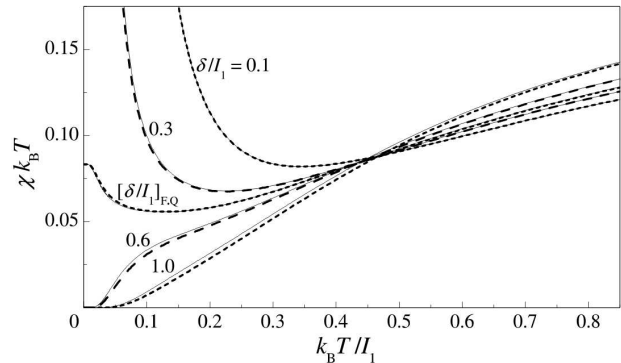

Fig. 5. Zero field magnetic susceptibility times the temperature as a function of the temperature for two points $(\tilde{t}, \tilde{U})$ and several selected values of $\tilde{\delta}$. The results for $\tilde{t} = 1$ and $\tilde{U} = 55/12$ are depicted by solid lines, and the results for the special limit $\tilde{U} \to \infty$ ($\tilde{J} = 0.75$) is depicted by dashed lines
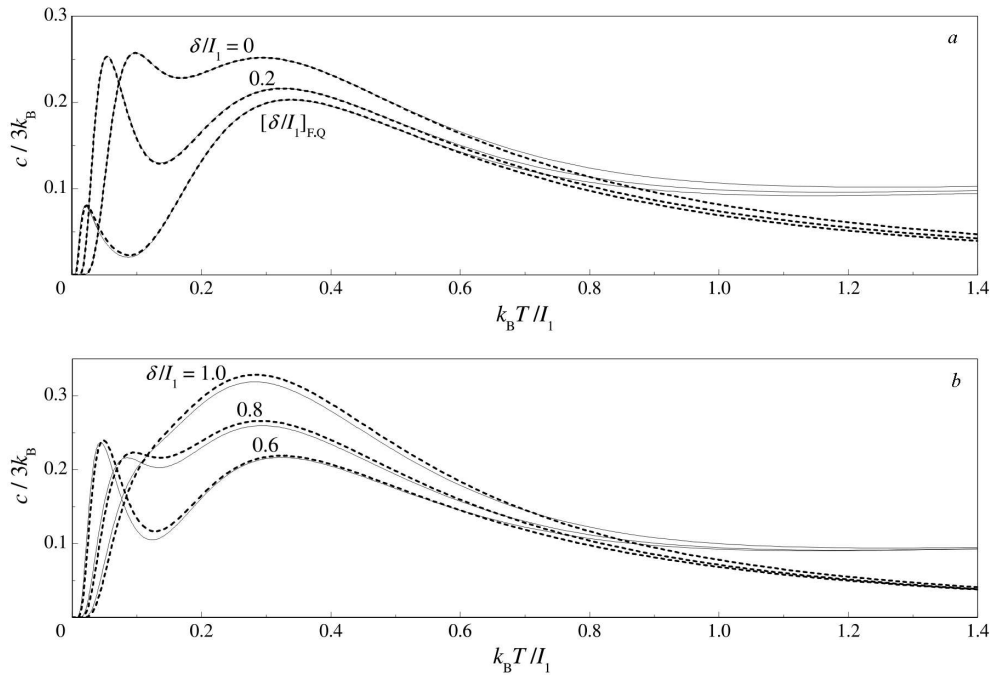

Fig. 6. Zero field specific heat as a function of the temperature for two points $(\tilde{t}, \tilde{U})$ and several selected values of $\tilde{\delta}$: on the interval $\tilde{\delta} \in [0, \tilde{\delta}_{\mathrm{F.Q}}]$ (a), which corresponds to the FRI ground state, and on the interval $\tilde{\delta} \in (\tilde{\delta}_{\mathrm{F.Q}}, 1]$ (b), which corresponds to the QAF ground state. The results for $\tilde{t} = 1$ and $\tilde{U} = 55/12$ are presentted by solid lines, and the result for the special limit $\tilde{U} \to \infty$ ($\tilde{J} = 0.75$) is given by dashed lines

topological line $\tilde{\mathcal{T}} = 1.5$: first point ($\tilde{t} = 1$, $\tilde{U} = 55/12 \approx 4.6$) and second point ($\tilde{t} = 10^3$, $\tilde{U} = 63999991/12 \approx 5333333$), which corresponds to the mathematical special limit $\tilde{U} \to \infty$ at $\tilde{J} = 0.75$. The temperature dependence of magnetization m for these two points $(\tilde{t}, \tilde{U})$ is presented in Fig. 4. We see that the temperature curves of magnetization for $\tilde{U} = 55/12$ and $\tilde{U} \to \infty$ practically coincide with each

other in the region of low and medium temperatures for all selected values of the magnetic field, except for the value $\tilde{h} = 0.3109$. The significant difference in temperature curves of magnetization at $\tilde{h} = 0.3109$ near zero temperature caused by the fact that for $\tilde{U} = 55/12$ the value $\tilde{h} = 0.3109$ belongs to the line of coexistence of QAF and FRI states, and for the special limit $\tilde{U} \to \infty$ it belongs to the region of the ground state QAF (Fig. 2). In the region of high temperatures, the magnetization curves for $\tilde{U} \to \infty$ lie somewhat higher than for $\tilde{U} = 55/12$.

In Fig. 5, we can see a slight quantitative difference between the temperature curves of the zero field magnetic susceptibility $\chi = \frac{dm}{dh}$ for $\tilde{U} = 55/12$ and $\tilde{U} \to \infty$, which are presented for several values of the parameter $\tilde{\delta}$. Note that the temperature curves $\chi k_{\mathrm{B}} T$ in Fig. 5 for $\tilde{\delta} = \tilde{\delta}_{\mathrm{F.Q}}$, where $\tilde{\delta}_{\mathrm{F.Q}}$ is the point of coexistence of FRI and QAF states at the zero field (Fig. 2), which is a function of $\tilde{t}$ and $\tilde{U}$, correspond to different values of $\tilde{\delta}$, because $\tilde{\delta}_{\mathrm{F.Q}} = 0.40815$ for $\tilde{U} = 55/12$, but $\tilde{\delta}_{\mathrm{F.Q}} = 0.40$ for the limit $\tilde{U} \to \infty$.

The specific heat $c = -T \frac{\partial^2 f}{\partial T^2}$, where f is the free energy per primitive cell in the thermodynamic limit [19], depending on the temperature at zero field is shown in Fig. 6. As it is known from Ref. [19], the temperature curves of the zero field specific heat for $\tilde{t} = 1$, $\tilde{U} = 55/12$ and $\tilde{\delta} \in [0, 1]$ have a very broad maximum in the high-temperature region, its initial part can be seen in Fig. 6. The temperature of this specific heat maximum is proportional to the on-site repulsion. In the special limit $\tilde{U} \to \infty$ the specific heat does not have this maximum [2]. Therefore this specific heat maximum corresponds to an intensive increase/decrease in the realization of states

$$\prod_{i=1}^{N} |\pm\rangle_i \, \frac{1}{\sqrt{2}} \left(|\uparrow\downarrow, 0\rangle_i - |0, \uparrow\downarrow\rangle_i \right),$$

the energy of which in the zero field is equal to $\tilde{U}$, and in the special limit $\tilde{U} \to \infty$ corresponds to $\mathcal{E}'_6(\mu_i, \mu_{i+1})$ (7), and states with a high probability of two electrons being in the same position, the energy of which in the zero field is slightly different from $\tilde{U}$, and, in the special limit $\tilde{U} \to \infty$, corresponds to $\mathcal{E}'_5(\mu_i, \mu_{i+1})$ (7). In the region of low and medium temperatures, the specific heat curves for $\tilde{U} = 55/12$ and in the limit $\tilde{U} \to \infty$ practically coincide with each other for $\tilde{\delta} \leqslant \tilde{\delta}_{\mathrm{F.Q}}$ (Fig. 6, *a*), and are very close

to each other for $\tilde{\delta} > \tilde{\delta}_{\mathrm{F.Q}}$ (Fig. 6, *b*). We note once again that the parameter $\tilde{\delta}_{\mathrm{F.Q}}$ has different values for $\tilde{U} = 55/12$ and for the limit $\tilde{U} \to \infty$.

We also calculated the magnetization, magnetic susceptibility, and specific heat as a function of the temperature at the zero field for the point $\tilde{t} = 10$ and $\tilde{U} = 6391/12$ on the equitopological line $\tilde{\mathcal{T}} = 1.5$. The temperature curves of magnetization and magnetic susceptibility for $\tilde{U} = 6391/12$ practically coincide with the corresponding curves for the limit $\tilde{U} \to \infty$, and the temperature curves of specific heat for $\tilde{U} = 6391/12$ differ from the corresponding curves for the limit $\tilde{U} \to \infty$ only by a very broad maximum (it starts at $k_{\mathrm{B}} T / I_1 \approx 36$) in the high-temperature region.

4. Conclusions

The quantum mechanical and thermodynamic properties of the distorted diamond Ising–Hubbard chain are considered in the limit $(t \to \infty, U \to \infty)|_{4t^2/U=J}$ by analytic and numerical approaches. The special limit $U \to \infty$ for the matrix of the cell Hamiltonian of this chain is analytically obtained by separating the contribution from the two-electron Hubbard dimer and applying unitary transformations. As a result, it is demonstrated that the matrix of the cell Hamiltonian of the distorted diamond Ising–Hubbard chain [19] in the special limit $U \to \infty$ after adding the constant $(J/4)$ and discarding the subspace of two infinite energies is equal to the matrix of the cell Hamiltonian of the spin-1/2 distorted diamond Ising–Heisenberg chain [2] with the antiferromagnetic isotropic Heisenberg interaction J. This means that the analytic results for the quantum states and thermodynamic characteristics of the distorted diamond Ising–Hubbard chain [19] in the special limit $U \to \infty$ correspond to the spin-1/2 distorted diamond Ising–Heisenberg chain [2] in the case of antiferromagnetic isotropic Heisenberg interaction J.

The special limit $U \to \infty$ for the ground state phase diagram in the plane (distortion parameter, magnetic field) and thermodynamic characteristics of the distorted diamond Ising–Hubbard chain [19] is numerically calculated in the case of antiferromagnetic Ising interaction, in which this model has geometric frustration. We have shown that the equitopological line

$$\sqrt{U^2 + 16t^2} - U = 2J$$

for the ground state phase diagram ends at the limit point $(t \to \infty, U \to \infty)|_{4t^2/U=J}$. Therefore, on the equitopological line there is a very strong qualitative and quantitative relationship between the numerical results for the ground state phase diagram and for the thermodynamic characteristics of this Ising–Hubbard model [19] and the numerical results for the ground-state phase diagram and for the thermodynamic characteristics of the corresponding Ising–Heisenberg model [2] with antiferromagnetic isotropic Heisenberg interaction. This confirms the analysis of the qualitative and quantitative relationship between the numerical results for the ground state phase diagram and, for the thermal and magnetic characteristics at two points of the equitopological line, the point near the beginning of the equitopological line and the point corresponding to the mathematical limit $(t \to \infty, U \to \infty)|_{4t^2/U=J}$. Consequently, the relationship between the Hubbard interaction parameters and the Heisenberg antiferromagnetic interaction parameter given by the equation of the equitopological line makes it possible, based on the results for the ground state phase diagram and the thermodynamic characteristics of the spin-1/2 distorted diamond Ising–Heisenberg chain with the antiferromagnetic isotropic Heisenberg interaction, to predict qualitative and quantitative behavior of the characteristics of the distorted diamond Ising–Hubbard chain.

It is worthwhile to remark that the obtained results are also valid for the Ising–Hubbard simple chain (Ising spins and two-electrons dimers are located on the line), in which the Ising spin is coupled with the first (I_1) and second (I_2) neighbors.

1. L. Čanová, J. Strečka, M. Jaščur. Geometric frustration in the class of exactly solvable Ising–Heisenberg diamond chains. *J. Phys.: Condens. Matter* **18**, 4967 (2006).

2. B.M. Lisnii. Spin-1/2 asymmetric diamond Ising–Heisenberg chain. *Ukr. J. Phys.* **56**, 1237 (2011).

3. N.S. Ananikian, L.N. Ananikyan, L.A. Chakhmakhchyan, O. Rojas. Thermal entanglement of a spin-1/2 Ising–Heisenberg model on a symmetrical diamond chain. *J. Phys.: Condens. Matter* **24**, 256001 (2012).

4. O. Rojas, M. Rojas, N.S. Ananikian, S.M. de Souza. Thermal entanglement in an exactly solvable Ising-XXZ diamond chain structure. *Phys. Rev. A* **86**, 042330 (2012).

5. N. Ananikian, V. Hovhannisyan. Magnetic properties, Lyapunov exponent and superstability of the spin-$\frac{1}{2}$ Ising–Heisenberg model on a diamond chain. *Physica A* **392**, 2375 (2013).

6. L. Gálisová. Magnetic properties of the spin-1/2 Ising–Heisenberg diamond chain with the four-spin interaction. *Phys. Status Solidi B* **250**, 187 (2013).

7. S. Bellucci, V. Ohanyan. Correlation functions in one-dimensional spin lattices with Ising and Heisenberg bonds. *Eur. Phys. J. B* **86**, 446 (2013).

8. J. Torrico, M. Rojas, S.M. de Souza, O. Rojas, N.S. Ananikian. Pairwise thermal entanglement in the Ising-XYZ diamond chain structure in an external magnetic field. *EPL* **108**, 50007 (2014).

9. L. Gálisová. Magnetocaloric effect in the spin-1/2 Ising–Heisenberg diamond chain with the four-spin interaction. *Condens. Matter Phys.* **17**, 13001 (2014).

10. N.S. Ananikian, V.V. Hovhannisyan, R. Kenna. Partition function zeros of the antiferromagnetic spin-$\frac{1}{2}$ Ising–Heisenberg model on a diamond chain. *Physica A* **396**, 51 (2014).

11. B. Lisnyi, J. Strečka. Exact results for a generalized spin-1/2 Ising–Heisenberg diamond chain with the second-neighbor interaction between nodal spins. *Phys. Status Solidi B* **251**, 1083 (2014).

12. V. Ohanyan, O. Rojas, J. Strečka, S. Bellucci. Absence of actual plateaus in zero-temperature magnetization curves of quantum spin clusters and chains. *Phys. Rev. B* **92**, 214423 (2015).

13. J. Torrico, M. Rojas, S.M. de Souza, O. Rojas. Zero temperature non-plateau magnetization and magnetocaloric effect in Ising-XYZ diamond chain structure. *Phys. Lett. A* **380**, 3655 (2016).

14. S.M. de Souza, O. Rojas. Quasi-phases and pseudo-transitions in one-dimensional models with nearest neighbor interactions. *Solid State Commun.* **269**, 131 (2017).

15. I.M. Carvalho, J. Torrico, S.M. de Souza, O. Rojas, O. Derzhko. Correlation functions for a spin-$\frac{1}{2}$ Ising-XYZ diamond chain: Further evidence for quasi-phases and pseudo-transitions. *Ann. Physics* **402**, 45 (2019).

16. T. Krokhmalskii, T. Hutak, O. Rojas, S.M. de Souza, O. Derzhko. Towards low-temperature peculiarities of thermodynamic quantities for decorated spin chains. *Physica A* **573**, 125986 (2021).

17. M.S.S. Pereira, F.A.B.F. de Moura, M.L. Lyra. Magnetization plateau in diamond chains with delocalized interstitial spins. *Phys. Rev. B* **77**, 024402 (2008).

18. M.S.S. Pereira, F.A.B.F. de Moura, M.L. Lyra. Magnetocaloric effect in kinetically frustrated diamond chains. *Phys. Rev. B* **79**, 054427 (2009).

19. B.M. Lisnii. Distorted diamond Ising–Hubbard chain. *Low Temp. Phys.* **37**, 296 (2011).

20. B.M. Lisnyi. Asymmetric diamond Ising–Hubbard chain with attraction. *Ukr. J. Phys.* **58**, 195 (2013).

21. M. Nalbandyan, H. Lazaryan, O. Rojas, S.M. de Souza, N. Ananikian. Magnetic, thermal, and entanglement

properties of a distorted Ising–Hubbard diamond chain. *J. Phys. Soc. Jpn.* **83**, 074001 (2014).

22. J. Torrico, M. Rojas, M.S.S. Pereira, J. Strečka, M.L. Lyra. Spin frustration and fermionic entanglement in an exactly solved hybrid diamond chain with localized Ising spins and mobile electrons. *Phys. Rev. B* **93**, 014428 (2016).

23. H. Kikuchi, Y. Fujii, M. Chiba, S. Mitsudo, T. Idehara, T. Kuwai. Experimental evidence of the one-third magnetization plateau in the diamond chain compound $Cu_3(CO_3)_2(OH)_2$. *J. Magn. Magn. Mater.* **272–276**, 900 (2004).

24. H. Kikuchi, Y. Fujii, M. Chiba, S. Mitsudo, T. Idehara, T. Tonegawa, K. Okamoto, T. Sakai, T. Kuwai, H. Ohta. Experimental observation of the 1/3 magnetization plateau in the diamond-chain compound $Cu_3(CO_3)_2(OH)_2$. *Phys. Rev. Lett.* **94**, 227201 (2005).

25. H. Kikuchi, Y. Fujii, M. Chiba, S. Mitsudo, T. Idehara, T. Tonegawa, K. Okamoto, T. Sakai, T. Kuwai, K. Kindo, A. Matsuo, W. Higemoto, K. Nishiyama, M. Horvatić, C. Bertheir. Magnetic properties of the diamond chain compound $Cu_3(CO_3)_2(OH)_2$. *Prog. Theor. Phys. Suppl.* **159**, 1 (2005).

26. K.C. Rule, A.U.B. Wolter, S. Süllow, D.A. Tennant, A. Brühl, S. Köhler, B. Wolf, M. Lang, J. Schreuer. Nature of the spin dynamics and 1/3 magnetization plateau in azurite. *Phys. Rev. Lett.* **100**, 117202 (2008).

27. H. Jeschke, I. Opahle, H. Kandpal, R. Valenti, H. Das, T. Saha-Dasgupta, O. Janson, H. Rosner, A. Brühl, B. Wolf, M. Lang, J. Richter, S. Hu, X. Wang, R. Peters *et al.* Multistep approach to microscopic models for frustrated quantum magnets: the case of the natural mineral azurite. *Phys. Rev. Lett.* **106**, 217201 (2011).

28. A. Honecker, S. Hu, R. Peters, J. Richter. Dynamic and thermodynamic properties of the generalized diamond chain model for azurite. *J. Phys.: Condens. Matter* **23**, 164211 (2011).

29. O. Derzhko, O. Krupnitska, B. Lisnyi, J. Strečka. Effective low-energy description of almost Ising–Heisenberg diamond chain. *EPL* **112**, 37002 (2015).

30. T. Verkholyak, J. Strečka. Modified strong-coupling treatment of a spin-$\frac{1}{2}$ Heisenberg trimerized chain developed from the exactly solved Ising–Heisenberg diamond chain. *Phys. Rev. B* **103**, 184415 (2021).

31. M. Takahashi. Half-filed Hubbard model at low temperature. *J. Phys. C* **10**, 1289 (1977).

32. A.H. MacDonald, S.M. Girvin, D. Yoshioka. $\frac{t}{U}$ expansion for the Hubbard model. *Phys. Rev. B* **37**, 9753 (1988).

Б.М. Лісний

РОМБІЧНОПОДІБНИЙ ЛАНЦЮЖОК ІЗІНГА–ГАББАРДА У СПЕЦІАЛЬНІЙ ГРАНИЦІ НЕСКІНЧЕННОГО ОДНОЦЕНТРОВОГО ВІДШТОВХУВАННЯ

Точний розв'язок для дисторсного ромбічного ланцюжка Ізінга–Габбарда аналізується в спеціальній границі нескінченного одноцентрового електрон-електронного відштовхування, де двоелектронний димер Габбарда стає еквівалентним антиферомагнітному ізотропному димеру Гайзенберґа. Аналітично розраховано спеціальну границю нескінченного відштовхування для матриці коміркового гамільтоніана цієї моделі і показано, що точний розв'язок для дисторсного ромбічного ланцюжка Ізінга–Габбарда в цій границі збігається з точним розв'язком спін-1/2 дисторсного ромбічного ланцюжка Ізінга–Гайзенберґа з антиферомагнітною ізотропною взаємодією Гайзенберґа. Чисельний розрахунок спеціальної границі нескінченного відштовхування для фазової діаграми основного стану і термодинамічних характеристик дисторсного ромбічного ланцюжка Ізінга–Габбарда виконано таким чином, щоб забезпечити дуже швидку збіжність до граничних результатів для цих характеристик.

К л ю ч о в і   с л о в а: ромбічний ланцюжок Ізінга–Габбарда, основний стан, точний розв'язок, термодинамічні характеристики, геометрична фрустрація.